Aalborg Universitet

Coal and Biomass Cofiring

CFD Modeling

Yin, Chungen

Published in:
New Trends in Coal Conversion

DOI (link to publication from Publisher):
[10.1016/B978-0-08-102201-6.00004-2](#)

Publication date:
2019

[Link to publication from Aalborg University](#)

Chapter 4: Coal and biomass co-firing: CFD modeling

Chungen Yin

Department of Energy Technology, Aalborg University, 9220 Aalborg East, Denmark

Tel.: +45 3062 2577. Email: chy@et.aau.dk

Abstract: Suspension-firing, fluidized bed combustion and grate-firing are the three main technologies used to co-fire coal and biomass for heat and power generation. Computational Fluid Dynamics (CFD) modeling is a powerful and cost-effective tool for problem-shooting, design and optimization and plays a vital role in the development of these co-firing technologies. This chapter focuses on CFD of coal and biomass co-firing. After a brief overview of the status of co-firing, the chapter presents in detail the basic modules in general co-firing CFD. Then, the specific or new modeling strategies and issues that are pertinent to each of co-firing technologies are elaborated. Finally, new modeling issues for coal and biomass co-firing under oxy-fuel conditions are presented, before concluding remarks on coal and biomass co-firing modeling are summarized.

1. Introduction

As an abundant, renewable and environmentally friendly energy resource, biomass and its co-firing with coal for heat and power generation has gained increasingly widespread concerns and also advanced a remarkable progress and development worldwide. In the design and optimization of all the biomass co-firing processes and technologies under different firing conditions, CFD modeling has played and will continue to play a vital role.

This chapter mainly focuses on CFD modeling of coal and biomass co-firing. First, the basic modules in general co-firing CFD are presented. Then, the specific or new modeling

strategies or issues associated with different combustion technologies or combustion conditions (e.g., air-fuel or oxy-fuel) are discussed. A balance between the breadth and depth is made in the chapter, aiming to attain both a good overview and an in-depth understanding of the modeling strategies and issues for coal and biomass co-firing.

2. An overview of coal and biomass co-firing

Biomass offers carbon-neutral flexible power generation at low capital cost regardless of weather conditions. Globally, biomass co-firing has been applied in more than 240 power plants, in which 48%, 24%, 19% and 9% are equipped with suspension-firing, bubbling fluidized bed (BFB), circulating fluidized bed (CFB) and grate boilers, respectively (IEA, 2017). The key features, pros and cons of these coal and biomass co-firing technologies are summarized in (Yin and Li, 2017). In Europe, current economic circumstances also favor a change to biomass co-firing as a partial solution for power generators (Lavery, 2013), and suspension-firing has witnessed great success in co-firing of woody biomass at low thermal shares (Al-Mansour and Zuwala, 2010). In the development of the coal and biomass co-firing technologies, CFD has been proven to be a powerful tool for increased understanding, exploration of unfamiliar conditions, design, problem-shooting and optimization of combustion processes (Kitto and Stultz, 2005; Yin et al. 2008a; Yin and Yan, 2016).

3. CFD modeling of coal and biomass co-firing: The basic and generic modules

For dilute multiphase reacting flows as seen in suspension co-firing systems and in the freeboard in both grate-fired boilers and fluidized bed combustion boilers, Eulerian-Lagrangian approach is commonly used in CFD modeling. The fluid transport equations are numerically solved in the Eulerian framework while the reacting fuel particles are tracked in the Lagrangian framework, both of which are closely coupled to each other. Figure 1 shows the overall structure and the key modules of CFD modeling of solid fuel combustion. When biomass is co-fired, pollutant formation (e.g., NO_x emissions) and ash

deposition also become important for the performance of the co-firing systems, primarily due to the low ash melting temperatures of most biomass fuels. The general modeling issues outlined in the seven bubbles are elaborated below.

Figure 1

3.1 Turbulent mixing

Industrial co-firing processes always feature a turbulent flow. Mainly limited by the computational resources, the major concerns of industrial co-firing CFD modeling are still placed on the mean flow characteristics. Therefore, time-averaging is widely used to eliminate turbulent fluctuations. The time-averaging of the fluid conservation equations introduces extra turbulent flux terms, making the system of the equations no longer closed. Turbulence models are needed. The commonly used turbulence models under the Reynolds-averaged Navier-Stokes (RANS) modeling framework assume the Reynolds or turbulent stresses are analogous to the viscous stresses. Such turbulence models account for the impact of the unresolved large-scale eddies on the mean fluid flow to some extent and close the system of time-averaged fluid transport equations.

With the advancement in computational power, large eddy simulation (LES) of coal and biomass co-firing has received great interest from academia in the last decade, which also spreads to industries now (Pitsch, 2006; Rabacal et al., 2014; Olenik et al., 2015). Different from the RANS modeling, in which only the mean flow quantities are resolved and the impact of the large-scale eddies on the mean flow is modeled, LES directly resolves the large-scale motion of the turbulence. The large-scale eddies, whose motion depends on the flow geometry, carry most of the turbulent kinetic energy and control the dynamics of the turbulence. In LES, only the small-scale sub-grid eddies, which are universal and not dependent on individual flow geometry, are modeled in order to account for their impact on the resolved large-scale eddies. As a result, LES, combined

with appropriate sub-grid models for the small-scale eddies, greatly outperforms RANS simulation in terms of accuracy, at the expenses of computational efficiency.

In a combustion furnace, turbulence plays the central role in mixing, and then in heat and mass transfer as well as chemical reactions. Accurate modeling of turbulence is very important. From this point of view, one can expect an eventual switch from RANS turbulence modeling to LES even for industrial co-firing CFD.

3.2 Fuel particle motion

Correct prediction of fuel particle trajectory in a furnace is important for air supply and combustion performance. The particle tracking model most commonly used in CFD is for small, heavy particles in dilute two-phase flows, for which it is sufficient to only retain drag and gravity forces in the equation of motion of particles (Maxey and Riley, 1983),

$$m_p \frac{d\mathbf{v}}{dt} = \underbrace{\tfrac{1}{2}C_D \rho_g A_p |\mathbf{u}-\mathbf{v}|(\mathbf{u}-\mathbf{v})}_{\text{drag,} \mathbf{F}_D} + \underbrace{(\rho_p - \rho_g)V_p \mathbf{g}}_{\text{gravity}} \tag{1}$$

where m_p, $\mathbf{v}$, t, C_D, ρ_g, A_p, $\mathbf{u}$, ρ_p, V_p and $\mathbf{g}$ represent particle mass, particle velocity vector, time, drag coefficient, gas density, particle projection area normal to the drag force, gas velocity vector, particle density, particle volume, gravitational acceleration, respectively. This model is applicable to and is also commonly used in suspension-firing of pulverized coal particles. However, in biomass co-firing, this model framework may have to be extended to accommodate the relatively large and highly non-spherical biomass particles, which will be elaborated in detail in section 4.2.

In turbulent multiphase flows, the interaction between turbulent eddies and immersed particles, known as turbulent particle dispersion, can be important. From the modeling point of view, the turbulent particle dispersion can be addressed by using either cloud tracking or stochastic tracking model. In the former, the mean fluid velocity $\mathbf{u}$ is used in Eq. (1) to obtain a mean trajectory, and the dispersive effect around the mean trajectory is described by an assumed probability density function. In the latter, a random fluid

velocity fluctuation $\mathbf{u}'$ following a certain profile is added to the mean fluid velocity $\mathbf{u}$ to update the particle velocity and position at the current time step. At the next time step, a new random velocity $\mathbf{u}'$ will be used, until the particle tracking is finished.

3.3 Radiation heat transfer

Thermal radiation is often the dominant heat transfer mechanism in combustion furnaces. For a gray participating medium containing particles, the radiative transfer equation (RTE) can be expressed as (Modest, 2003),

$$\frac{dI}{ds} = \underbrace{\alpha \frac{\sigma T_g^4}{\pi}}_{\text{gas emission}} + \underbrace{\sum_i \varepsilon_{p,i} n_i A_{p,i} \frac{\sigma T_{p,i}^4}{\pi}}_{\text{particle emission}} - \underbrace{(\alpha + \alpha_p + \sigma_p) I}_{\text{absorption/scattering losses}} + \underbrace{\frac{\sigma_p}{4\pi} \int_{4\pi} \phi(\hat{s}' \Rightarrow \hat{s}) I \, d\Omega'}_{\text{in-scattering gain}} \quad (2)$$

in which $I(\vec{r}, \hat{s})$, s, α, σ, T_g, $\varepsilon_{p,i}$, n_i, $A_{p,i}$, $T_{p,i}$, α_p, σ_p and $\phi(\hat{s}' \Rightarrow \hat{s})$ represent the radiative intensity at position $\vec{r}$ in direction $\hat{s}$, path length, local gas absorption coefficient, Stefan-Boltzmann constant, local gas temperature, emissivity of group i particles, number density of group i particles, projected area of group i particles, temperature of group i particles, particle absorption coefficient, particle scattering coefficient, and phase function for radiation beam in $\hat{s}'$ direction being scattered into $\hat{s}$ direction, respectively. The gas absorption coefficient and the particle absorption and scattering coefficients are calculated by (Chui et al., 1993),

$$\alpha = -(1/L) \cdot \ln(1 - \varepsilon) \quad (3)$$

$$\alpha_p = \sum_i \varepsilon_{p,i} n_i A_{p,i} \quad (4)$$

$$\sigma_p = \sum_i (1 - f_{p,i})(1 - \varepsilon_{p,i}) n_i A_{p,i} \quad (5)$$

in which L, ε and $f_{p,i}$ are the domain-based beam length, total emissivity of local gas mixture, and scattering factor of group i particles, respectively. In combustion CFD, the total gas emissivity ε is often calculated by a weighted sum of gray gases model (WSGGM) while different constants are usually used for particle emissivity ε_p and particle scattering factor f_p.

Given the gas and particle radiative properties, the RTE, Eq. (2), can be numerically solved for the radiative intensity $I(\vec{r}, \hat{s})$. In solid fuel combustion CFD, the Discrete Ordinates (DO) and P1 models are commonly used to solve the RTE. The former is applicable to all optimal thicknesses but is computationally expensive; while the latter is computationally cheap but only applicable to optically thick participating medium (i.e., large-scale boilers). Once the radiative intensity I is solved, the heat source due to radiation in the energy transport equation can be evaluated by,

$$-\nabla \cdot q_r = -4\pi \left(\alpha \frac{\sigma T_g^4}{\pi} + \sum_i \varepsilon_{p,i} n_i A_{p,i} \frac{\sigma T_{p,i}^4}{\pi} \right) + (\alpha + \alpha_p) \int_{\Omega=4\pi} I(\vec{r}, \hat{s}) d\Omega \quad (6)$$

in which q_r and Ω denote the radiative flux and solid angle, respectively

3.4 Heterogeneous reactions

When travelling through gas and interacting with gas in the furnace, the fuel particles heat up, and undergo a series of heterogeneous reactions such as pyrolysis and char oxidation and gasification, creating sources for reactions in gas phase.

3.4.1 Pyrolysis

Pyrolysis, occurring at the early stage of solid fuel combustion, plays a key role in a combustion process. It controls the yields of volatiles, tars and char, determines the split of fuel nitrogen into volatiles and char, and affects the physical properties of the resultant char. Therefore, ignition, flame stability, char burnout and pollutant formation are all affected. Proper modeling of the pyrolysis process is important in co-firing CFD. As reviewed in (Yu et al., 2007), there are different pyrolysis models, e.g.,

- the single kinetic rate model, assuming the pyrolysis rate is first-order dependent on the amount of volatiles left in the particle (Badzioch and Hawksley, 1970),
- the two competing rates model, in which two different kinetic rates control the pyrolysis over different temperature ranges (Kobayashi et al., 1976),
- various network pyrolysis models which do not rely on Arrhenius rate relations, e.g., the Chemical Percolation Devolatilization model (Grant et al., 1989), the

Functional Group - Depolymerisation Vaporisation Cross-linking model (Solomon et al., 1988), and the FLASHCHAIN model (Niksa and Kerstein, 1991).

Among these models, the most commonly used model is still the single kinetic rate model. Due to the lack of data, the Arrhenius rate parameters are often taken from the literature. They are better determined experimentally or even estimated by network pyrolysis codes, because the pyrolysis kinetic data are dependent on the fuel properties and pyrolysis conditions and the literature data are not likely to be general.

3.4.2 Char reactions

Char oxidation and gasification is another group of heterogeneous reactions, occurring at the relatively late stage of solid fuel combustion. There are different gas species in the boundary layer around the solid char particle surface, e.g., O_2, CO_2 and H_2O, which could result in global heterogeneous reactions on the char particle surface:

$$C + 0.5O_2 \rightarrow CO \tag{R1}$$

$$C + O_2 \rightarrow CO_2 \tag{R2}$$

$$C + CO_2 \rightarrow 2CO \tag{R3}$$

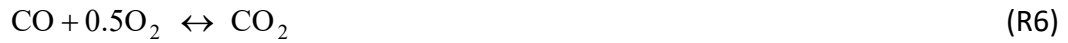$$C + H_2O \rightarrow H_2 + CO \tag{R4}$$
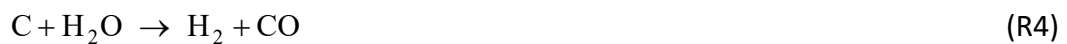
From modeling point of view, different approaches exist for char reactions, e.g.,

- One-film model: There is no flame in the gas phase. Char is directly oxidized into CO_2 at the particle surface. As a result, both the temperature and CO_2 peak at the particle surface and decay when moving away from the particle surface.

- Two-film model: the principal product at the char particle surface is CO. CO diffuses always from the particle surface and reacts with inward-diffusing O_2, $CO+0.5O_2 \rightarrow CO_2$, forming a visible flame at a distance away from the surface.

- Continuous-film model: a flame zone is distributed within the boundary layer around the char particle, rather than occurring in one or two sheets.

The one-film model is most widely used for char reactions in solid fuel combustion CFD, in which different char surface reaction regimes can be identified: kinetics-controlled (zone I), diffusion- and kinetics-controlled (zone II), and diffusion-controlled (zone III).

3.5 Homogeneous reactions

In coal and biomass co-firing, the combustion of the released volatiles plays a vital role in ignition, local stoichiometry, flame stability and pollutant formation. Therefore, gas-phase reaction modelling is also important. The overwhelming majority of industrial combustion CFD relies on global combustion mechanisms. The commonly used global mechanisms include the two-step hydrocarbon oxidation mechanism by Westbrook and Dryer (WD) (Westbrook and Dryer, 1981; Westbrook and Dryer, 1984) and the four-step mechanism developed by Jones and Lindstedt (JL) (Jones and Lindstedt, 1988) for alkane hydrocarbons up to butane in mixtures with air in premixed and diffusion flames. Taking CH_4 as an example, the WD 2-step mechanism is,

$$CH_4 + 1.5O_2 \rightarrow CO + 2H_2O \tag{R5}$$

$$CO + 0.5O_2 \leftrightarrow CO_2 \tag{R6}$$

And the JL-4 step scheme reads,

$$CH_4 + 0.5O_2 \rightarrow CO + 2H_2 \tag{R7}$$

$$CH_4 + H_2O \rightarrow CO + 3H_2 \tag{R8}$$

$$H_2 + 0.5O_2 \leftrightarrow H_2O \tag{R9}$$

$$CO + H_2O \leftrightarrow CO_2 + H_2 \tag{R10}$$

which includes two competing fuel breakdown reactions into CO and H_2 and two reversible reactions controlling the rate of reactions for CO and H_2.

For non-premixed combustion, the thermochemistry can be reduced under certain assumptions to a single conserved parameter: the mixture fraction. The mixture fraction is the mass fraction of the elements that originate from the fuel stream. Since the mixture fraction is a conserved scalar, its governing transport equation does not have a source term, eliminating the difficulties associated with modeling the nonlinear mean reaction rates in the species transport equations. By using mixture fraction approach for non-premixed combustion, combustion is simplified to a mixing problem. Once mixed, the instantaneous species fractions, density and temperatures can be related to the calculated mixture fractions by using detailed kinetic mechanisms, e.g., the equilibrium

model, steady diffusion flamelet model, or unsteady diffusion flamelet model. Then, the time-averaged values of the parameters such as species and temperature are evaluated from the instantaneous values and an assumed probability density function (PDF).

3.6 Pollutant formation

NO_x in combustion processes can be formed via thermal NO_x (by oxidation of N_2 in the oxidizer at temperatures above 1800 K), prompt NO_x (by hydrocarbon radicals attacking N_2 to form cyanide species and then to NO at the flame front), and fuel NO_x (by oxidation of nitrogen contained in the fuel). For conventional air-fuel combustion of pulverized coal, the majority of the total NO_x is from fuel NO_x and up to 20% is due to thermal NO_x while the prompt NO_x is negligible (Glarborg et al., 2003).

3.6.1 Thermal NO_x

Thermal NO_x formation can be modeled by the extended Zeldovich mechanism (Miller and Bowman, 1989; Zeldovich, 1946):

$$O + N_2 \ \leftrightarrow \ N + NO \tag{R11}$$

$$N + O_2 \ \leftrightarrow \ O + NO \tag{R12}$$

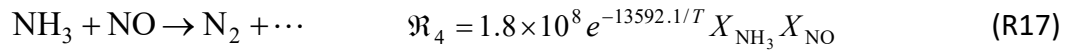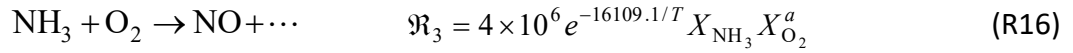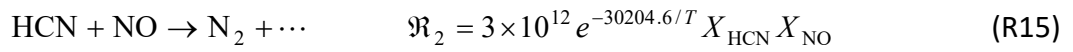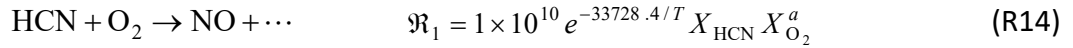$$N + OH \ \leftrightarrow \ H + NO \tag{R13}$$
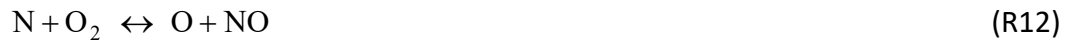
from which the net rate of formation of NO is expressed in terms of the kinetics of the three reactions and the O, H, OH and N concentrations. A quasi-steady assumption for [N], i.e., the consumption rate of free N atoms equals to its formation rate, is often used to simplify the expression of the net formation rate of thermal NO in terms of the kinetics of the three reactions and the concentrations of [O] and [OH]. The [O] and [OH] can be determined by either equilibrium approach or partial equilibrium approach. The thermal NO_x modeling is often decoupled from the main combustion process with frozen field of temperature, stable species, [O] and [OH]. Once the net rate of formation is calculated, the NO source term due to thermal NO_x mechanism can be evaluated by,

$$S_{\text{Thermal NOx}} = \left(\frac{d[NO]}{dt} \right)_{\text{thermal}} \cdot MW_{NO} \tag{7}$$

in which MW_{NO} is the molecular weight of NO.

3.6.2 Fuel NOₓ

Fuel NO$_x$ can be formed via different pathways as shown in Fig. 2 (Hill and Smoot, 2000; Glarborg et al., 2003; Yin et al., 2008a). During pyrolysis, the volatile-N is released together with the majority of volatiles. The NO$_x$ precursors, mainly HCN and NH$_3$, are competitively oxidized to NO and reduced to N$_2$ (De Soete, 1975):

$$HCN + O_2 \rightarrow NO + \cdots \qquad \Re_1 = 1 \times 10^{10} e^{-33728.4/T} X_{HCN} X_{O_2}^a \qquad (R14)$$

$$HCN + NO \rightarrow N_2 + \cdots \qquad \Re_2 = 3 \times 10^{12} e^{-30204.6/T} X_{HCN} X_{NO} \qquad (R15)$$

$$NH_3 + O_2 \rightarrow NO + \cdots \qquad \Re_3 = 4 \times 10^6 e^{-16109.1/T} X_{NH_3} X_{O_2}^a \qquad (R16)$$

$$NH_3 + NO \rightarrow N_2 + \cdots \qquad \Re_4 = 1.8 \times 10^8 e^{-13592.1/T} X_{NH_3} X_{NO} \qquad (R17)$$

in which $\Re$, T and X denote the conversion rate (s^{-1}), temperature in (K) and mole fractions, respectively. Based on these reaction rates, the source terms in the transport equations for HCN, NH$_3$ and NO due to volatile-N conversion can be readily evaluated, among which the NO source term is,

$$S_{volatile,NO} = (\Re_1 - \Re_2 + \Re_3 - \Re_4) \cdot MW_{NO} \cdot P/(R_u \cdot T) \qquad (8)$$

where P and R_u denote the pressure and universal gas constant, respectively.

Figure 2

For char-N conversion, most of the char-N is oxidized to NO as a desorption product from the oxidized char-N atoms (Lockwood and Romo-Millares, 1992), and the rest is converted to N$_2$, if neglecting char-N conversion to the NO$_x$ precursors. The NO source due to char-N oxidation is calculated as,

$$S_{char,NO} = \frac{S_c Y_{N,char} MW_{NO}}{MW_N \cdot V} \eta \qquad (9)$$

where S_c, $Y_{N,char}$, V, η and MW_N represent the char burnout rate (kg/s), mass fraction of nitrogen in char, cell volume (m³), conversion factor, molecular weight of N

(kg/kmol), respectively. The conversion factor, η, is to account for that some of the char-N is converted to N$_2$, as shown in Fig. 2.

The NO formed may be reduced to N$_2$ over the residual char due to its catalytic effect on NO formation and reduction. The NO reduction rate can be calculated as,

$$S_{\text{NO, reduction}} = c_s A_{\text{BET}} \, \text{MW}_{\text{NO}} \cdot 0.23 \, e^{-17166.3/T} X_{NO} P_{\text{atm}} \tag{10}$$

where c_s, A_{BET}, X_{NO} and P_{atm} are the fuel particle concentration (kg/m^3), particle BET surface area (m^2/kg), mole fraction of NO, and pressure (atm), respectively.

If neglecting the direct conversion fuel-N to NO$_x$, the NO source term due to fuel NO$_x$ mechanism can be summed up as follows,

$$S_{\text{Fuel NOx}} = S_{\text{volatile,NO}} + S_{\text{char,NO}} - S_{\text{NO,reduction}} \tag{11}$$

Compared to thermal NO$_x$ which depends on the main combustion simulation results such as temperature and oxygen, fuel NO$_x$ prediction also relies on

- the fuel-N split ratio in volatiles and char.
- the volatile-N partitioning for HCN and NH$_3$. For low-ranking (lignite) coal and biomass, NH$_3$ is the major NO$_x$ precursor; while for higher-ranking (bituminous) coals, HCN is the major precursor.
- the conversion factor of char-N to NO, η. The contribution of char-N to the NO$_x$ precursors is often neglected. If also neglecting char-N conversion to N$_2$, a conversion factor of char-N to NO, $\eta = 1$, can be used.

3.7 Ash behavior

In coal/biomass co-firing, non-combustible material in the fuel such as fly ash particles and salt vapors may be deposited on wall surfaces in a boiler. When wall surface temperatures are lower than local gas temperatures, the alkali salt vapors may be condensed to form sub-micron droplets/particles in the boundary layer close to the walls and get deposited on the wall surfaces. After the initial condensed deposit is

formed, the large and intermediate-sized particles start to stick on the wall surfaces. Modeling of ash deposition in solid fuel combustion often considers the following mechanisms (Baxter, 1993; Wang and Harb, 1997; Lee and Lockwood, 1999; Kær et al., 2006; Weber et al., 2013).

- For the sub-micron salt vapor droplets/particles, the deposit is formed mainly via diffusion, turbulent eddy-impaction, and thermophoretic mechanisms.
- For fly ash particles, the deposit is formed mainly by inertial impaction, while turbulent and thermophoretic mechanisms also contribute to some extent.

The deposition velocity $u_d = \dot{m}_d'' / C_0$ is often normalized by the friction velocity or shear velocity u_τ to yield a dimensionless deposition velocity u_d^+,

$$u_d^+ = \frac{u_d}{u_\tau} = \frac{\dot{m}_d'' / C_0}{\sqrt{\tau_w / \rho_g}} \tag{12}$$

where $\dot{m}_d''$, C_0, τ_w and ρ_g represents particle deposition flux (kg/(m²·s)), near-wall droplet/particle mass concentration (kg/m³), wall shear stress (Pa), and gas density at wall temperature (kg/m³), respectively. Empirical correlations for the dimensionless deposition velocity exist in literature.

For sub-micron salt vapor droplets/particles, the dimensionless deposition velocities due to diffusion, turbulent eddy-impaction, and thermophoretic mechanisms are,

$$\begin{cases} u_{d,Diff}^+ = 0.057\, Sc_p^{-2/3} \\ u_{d,Turb}^+ = \min\!\left(4.5 \times 10^{-4} (\tau_p^+)^2,\, 0.14\right) \\ u_{d,Therm}^+ = (F_{therm} \cdot \tau_p)/(m_p \cdot u_\tau) \end{cases} \tag{13}$$

where Sc_p, τ_p^+, F_{therm}, τ_p and m_p are the particle Schmidt number, dimensionless particle relaxation time, thermophoretic force, particle relaxation time and particle mass, respectively. Based on the above empirical equations, the deposition rate of a given salt vapor, i, can be calculated as,

$$\dot{m}_{d,\,\text{vapor}\,i}'' = \underbrace{(u_{d,Diff}^+ + u_{d,Turb}^+ + u_{d,Therm}^+)}_{\text{total dimensionless deposition velocity}} \cdot u_\tau \cdot \underbrace{(\rho_g Y_{\text{vapor}\,i})}_{\text{mass concentration}} \tag{14}$$

in which the mass fraction of vapor i, $Y_{\text{vapor}\,i}$, is calculated from its transport equation.

For fly ash particles, the deposition rate is calculated as,

$$\dot{m}''_{d,\text{flyash}} = \underbrace{\dot{m}_p \cdot \eta_{stick} / A}_{\dot{m}''_{d,Inert}} + \underbrace{(u^+_{d,Turb} + u^+_{d,Therm}) \cdot u_\tau \cdot Conc_p \cdot \eta_{stick}}_{\dot{m}''_{d,Turb} + \dot{m}''_{d,Therm}} \tag{15}$$

where $\dot{m}_p$, A, η_{stick} and $Conc_p$ represent the mass flow rate of fly ash particles being tracked that is currently hitting a wall, area of the reflecting surface that the particle is hitting, net fraction of particles contributing to deposit growth which is dependent on both the particle and wall surface conditions (e.g., particle and wall temperatures), and particle mass concentration, respectively.

The total deposition rate are calculated as, $\dot{m}''_d = \dot{m}''_{d,\text{vapor }i} + \dot{m}''_{d,\text{flyash}}$, among which the inertial impaction of fly ash particles makes the major contribution while the empirical correlation of the sticking fraction η_{stick} is the main uncertainty.

Besides deposit formation mechanisms, deposit shedding can occur due to factors such as erosion, gravity shedding and thermal shock and need to be considered in deposition modeling. Empirical criteria and correlations are used for deposit shedding in modeling of superheater deposit formation in a biomass-fired grate boiler (Zhou at al., 2007).

4. Suspension co-firing of coal and biomass: CFD modeling

4.1 Biomass preparation for suspension-firing and overall modeling strategy

Suspension firing enjoys the popularity in coal and biomass co-firing: used in about half of the co-firing plants worldwide. The overall modeling strategy for suspension co-firing is same as the structure sketched in Figure 1. Compared to modeling of suspension firing of pulverized coal, a few special modeling issues arise in modeling of biomass suspension co-firing, mainly due to biomass preparation processes. In general, biomass preparation processes tend to produce relatively large, highly non-spherical particles, which have distinctly different motion and conversion patterns from tiny pulverized coal particles.

Figure 3

In the old preparation method, the raw biomass is transported to power plants and then handled and fired in the plants. Here, suspension co-firing of Danish wheat straw in a utility boiler at Studstrup power plant in Denmark is used as an example to illustrate the preparation process. The straw bales are first shredded in a shredder to obtain a continuous flow of straw, which then pass through a hammer mill after stones and the likes are separated. In the hammer mill, the straw are fragmented into small particles. Finally, the milled particles are pneumatically transported to the furnace for combustion. Because raw biomass are often fibrous and non-friable, it is hard for such a preparation process to obtain biomass particles of similar sizes as coal particles. Figure 3 shows the straw particle samples collected prior to injection into the boiler. The straw particles are large and highly non-spherical: a mean length of about 16 mm and a maximum length of 180 mm, as detailed in (Yin et al., 2004; Rosendahl et al., 2007).

Figure 4

Figure 5

In the latest retrofits for co-firing biomass in suspension-fired boilers, biomass pellets, rather than raw biomass, are transported to power plants and then milled and fired in the plants. For example, for biomass suspension co-firing in Amager unit 1 in Denmark (Mandø et al., 2010), the commercially available wood pellets from different suppliers are mixed in the silo and are ground in the traditional coal roller mills without changing any setting in the mills (as illustrated in Figure 4). Some roller-milled samples that are collected from the transport pipe to a burner in the plant are shown in Figure 4. The same wood pellets are also ground in hammer milling trials, as illustrated in Figure 5, in which some of the milled samples are shown.

Figure 6

Figure 6 shows an example of the cumulative particle size distribution measured by the conventional sieving analysis for the roller-milled and hammer-milled wood pellet samples. Milling of biomass pellets is found to result in much smaller particles than milling of raw biomass, and the hammer mill produces smaller particles than the conventional coal roller mill does. However, the biomass particles are still large in size and non-spherical in shape, which induces differences in modeling of biomass particle motion and conversion in a suspension-fired furnace.

4.2 Special modeling issue: Motion of large, non-spherical biomass particles

In the traditional method to model particle motion in suspension-fired furnaces, as described in Section 3.2, only translation motion is solved and only the drag and gravity force are retained in the equation of motion, assuming small, spherical, heavy particles in dilute two-phase flows. This is acceptable for conventional pulverized coal combustion. For large, highly non-spherical biomass particles shown in Figure 3, 4 and 5 as examples, such a traditional method is not applicable any more.

Instead, the coupled particle translation and rotation motion need to be solved. In the equation of translation, Eq. (16), all the important forces such as drag, lift, virtual mass and pressure gradient ($\mathbf{F}_D$, $\mathbf{F}_L$, $\mathbf{F}_{VM}$ and $\mathbf{F}_{PG}$) have to be included. In the equation of rotation, Eq. (17), all the important torques with respect to the three particle axes ($T_{x'}$, $T_{y'}$, $T_{z'}$), such as the torque induced by the aerodynamic forces and the resistance torque on a rotating body, need to be included. Since particle translation is described in the inertial coordinate ($\vec{x}$) while particle rotation is in the particle coordinate ($\vec{x'}$), a transformation matrix is needed to bridge the two coordinate systems.

$$m_p \frac{d\mathbf{v}}{dt} = \underbrace{\mathbf{F}_D + \mathbf{F}_L + \mathbf{F}_{VM} + \mathbf{F}_{PG}}_{\text{aerodynamic forces}} + \underbrace{(\rho_p - \rho_g)V_p \mathbf{g}}_{\text{gravity}} \qquad (16)$$

$$\begin{cases} I_{x'}\dfrac{d\omega_{x'}}{dt} - \omega_{y'}\omega_{z'}(I_{y'} - I_{z'}) = T_{x'} \\[2mm] I_{y'}\dfrac{d\omega_{y'}}{dt} - \omega_{z'}\omega_{x'}(I_{z'} - I_{x'}) = T_{y'} \\[2mm] I_{z'}\dfrac{d\omega_{z'}}{dt} - \omega_{x'}\omega_{y'}(I_{x'} - I_{y'}) = T_{z'} \end{cases} \qquad (17)$$

Such a model for tracking large, non-spherical particles in dilute two-phase flow is described in detail in (Yin et al., 2003). The model is validated by experiments, before it is refined for biomass co-firing modeling (Yin et al., 2004). Here, a few results are given as examples. Figure 7 shows the model-predicted and experiment-observed motion pattern of a cylindrical PVC particle (5.41 mm in diameter, 50 mm in length and 1366 kg/m^3 in density) released from rest in originally stagnant water, and the final water flow due to the coupling between the particle and the water. The cylindrical particle is found to have a remarkable lateral motion along its settling in the water tank.

Figure 7

4.3 Special modeling issue: Conversion of large biomass particles

A fuel particle experiences different sub-processes in its conversion, such as drying, pyrolysis, combustion of the released volatiles, and char reactions, as seen in Fig. 8(a). In the traditional modeling method, the sequential conversion pattern is used, by assuming particles under an isothermal condition, as illustrated in Fig. 8(b). Such an assumption may not be valid for large, highly non-spherical biomass particles, in which the different sub-processes can occur simultaneously, as seen in Fig. 8(c).

Figure 8

To investigate the impact of intra-particle heat and mass transfer on conversion of large biomass particles, a 1D particle conversion model is developed and implemented into coal/biomass suspension co-firing in a swirl-stabilized dual-feed burner flow reactor (Yin

et al., 2010a). The large fuel particle is discretized into some control volumes, on each of which the mass, energy and species equations are numerically solved. In conclusion, the simultaneous conversion model needs to be used for large particles whose sizes are on the order of millimeters or above. For biomass particles of a few hundred microns in diameter, the intra-particle heat and mass transfer may be a secondary issue at most in their conversion and the simplified sequential conversion model can be used.

5. Grate co-firing and fluidized bed co-firing of coal and biomass: CFD modeling

Grate-firing and fluidized bed combustion technologies contribute to another half of the co-firing plants worldwide. In both grate-fired boilers and fluidized bed boilers, there is a fixed, moving or fluidized dense bed of solid fuel particles in the bottom of the furnaces, making them distinctly different from suspension-fired boilers.

5.1 Overall modeling strategy

For grate-fired and fluidized bed boilers, the overwhelming majority of modeling work employs the Eulerian-Lagrangian approach, in which modeling of the freeboard zone in both grate-fired boilers and fluidized bed combustors is still the same as the structure sketched in Figure 1 while special attention is paid to modeling of the dense fuel bed. The two parts, i.e., modeling of fuel conversion in the dense fuel bed and modeling of dilute gas-solid flow reactions in the freeboard, are strongly coupled to each other by combustibles leaving the dense bed into the freeboard and radiative heat flux incident from the freeboard onto the fuel bed. As seen in Fig. 9, the coupled modeling strategy needs to iteratively switch between the dense fuel bed conversion modeling and the freeboard reacting flow simulation, until there is no remarkable change in both the combustibles leaving the fuel bed and the incident radiative heat flux onto the fuel bed.

Figure 9

5.2 Special modeling issue: Solid fuel conversion in a dense fuel bed

Different approaches exist for modelling of solid fuel conversion in a dense fuel bed.

In the first approach, the porous zone model of commercial CFD package can be used for the dense fuel bed conversion. The fuel bed itself can be included in CFD of the boiler (Collazo et al., 2012; Gómez et al., 2014) or be modeled separately (Nasserzadeh et al., 1991, 1993). In the former, the mass, momentum, species and energy source terms in the porous zone need to be properly evaluated and included in the transport equations. In the latter, the dense fuel bed is not a part of the CFD of the boiler and the results got from the porous zone model are used as the inlet conditions for the freeboard CFD.

In the second approach, empirical models are used to predict the conversion of the dense fuel bed. For example, the dense fuel bed is treated as a 0D system, in which the thermochemical processes are divided in two successive sections: drying and chemical conversion. Phenomenological laws are used to characterize the syngas release as a function of the main governing parameters (Costa et al., 2014). Modeling of the conversion of the dense bed in a grate-fired boiler can also be done by using an experience- or measurement-based conversion rates as a function of the position on the grate. Then, an overall heat and mass balance of fuel components and primary air can be solved to obtain the lengthwise profiles of temperature, species and velocity on the top of the dense fuel bed along the grate. Such profiles are used as the grate inlet conditions for the freeboard CFD (Blasiak et al., 2006; Goerner and Klasen, 2006; Kim et al., 1996; Klason and Bai 2006; Rajh et al., 2016; Stubenberger et al., 2008; Weissinger et al., 2004; Yin et al., 2008b, 2012).

In the third approach, separate comprehensive bed models are developed to study solid fuel conversion in a dense fuel bed. Basically, this approach is to numerically solve the mass, momentum, energy, and species conservation equations for gas and solid phases. Process rate equations and empirical correlations/sub-models are used for the closure

of the conservation equations. Such a comprehensive model can provide the profiles of all the parameters at the top of the dense bed, which can be used as the inlet boundary condition for the freeboard CFD (Goddard et al., 2005; Kær 2004; Ryu et al. 2002, 2004; Yang et al. 2007). Such a model also facilitates a parametric study of the impacts of feedstock properties, process conditions, and uncertainties in model assumptions and parameters on the conversion rate, temperature, and gas compositions (Thunman and Leckner, 2005; Zhou et al., 2005; Yang et al., 2005; Shin and Choi, 2000; Johansson et al., 2007). The majority of such comprehensive models are 1D, in which a 1D transient model is solved along the vertical direction for fixed bed combustion and then the time elapsed since ignition in the fixed bed is mapped to the horizontal distance away from the start point on the travelling grate in industrial grate boilers. Such an approximation may be acceptable for travelling grate combustion, because of the small gradients in temperatures and species along the horizontal direction in industrial grate boilers.

To gain a better overview of the comprehensive model (including the governing equations) and to develop a more general code for solid fuel combustion in a dense bed, MFIX (Multiphase Flow with Interphase eXchanges) is a useful reference. MFIX is a general-purpose computer code developed for describing the hydrodynamics, heat transfer, and chemical reactions in fluid–solid systems. MFIX code is based on a generally accepted set of multiphase flow equations as summarized in (Benyahia et al., 2012), and the source code is available via its website, https://mfix.netl.doe.gov. MFIX calculations give transient data on the 3D distribution of pressure, velocity, temperature, and species mass fractions. Though MFIX is mainly used for describing BFBs and CFBs and spouted beds, the governing equations and the programming techniques are still the same and useful for the development of dense fuel bed models for grate-fired boilers.

No matter which approach is used to model solid fuel conversion in a dense fuel bed, it is important to assure the correct total fluxes of mass, momentum, elements and heat released from the top of the dense bed into the freeboard in order to achieve a reliable CFD analysis of a grate-fired or a fluidized bed boiler. Compared to the correct total

fluxes into the freeboard, the different profiles of velocity, temperature and species along the top surface of the dense fuel bed produced by different approaches may be a secondary issue at most in the freeboard CFD. Due to the strong mixing in the freeboard in modern grate-fired boilers or fluidized bed combustors, the effect of the dense bed conversion models may be virtually restricted to the vicinity of the fuel bed.

6. Coal and biomass co-firing under oxy-fuel conditions: Special modeling issues

Oxy-fuel combustion has gained many concerns worldwide in the past years. More recently, oxy-fuel co-firing of coal and biomass also gains much attention, considering that a below-zero CO_2 emission may be achieved by combining the advantages of both oxy-fuel combustion and biomass co-firing. The use of CO_2 or the mixture of CO_2 and H_2O vapor as the diluent in oxy-fuel combustion, instead of N_2 in air-fuel combustion, induces significant changes to the combustion fundamentals, particularly to radiative heat transfer and combustion chemistry, as reviewed in (Yin and Yan, 2016).

Coal and biomass co-firing under oxy-fuel conditions has been numerically investigated in literature, e.g., (Álvarez et al., 2013, 2014; Bhuiyan and Naser, 2015, 2016; Black et al., 2013). The overall modeling strategy of oxy-fuel co-firing is same as that of air-fuel co-firing. Although the majority of the impacts of the combustion atmospheres can be accommodated in modeling naturally, efforts are still needed to refine the existing models or mechanisms for radiative heat transfer and gas phase combustion chemistry in order to make them applicable to oxy-fuel combustion (Yin and Yan, 2016).

6.1 Modeling of gaseous radiative properties under oxy-fuel conditions

The radiative transfer equation to be solved under a typical solid fuel combustor is presented in Eq. (2), in which the gas and particle radiative properties are evaluated by Eq. (3)-(5), respectively. The total gas emissivity of a local gas mixture to be used in Eq. (3), ε, is commonly evaluated by a weighted sum of gray gases model (WSGGM) in

combustion CFD, because it is a good compromise between computational efficiency and accuracy. The WSGGM postulates that the total emissivity may be represented by the sum of the emissivities of several hypothetical gray gases and one clear gas, weighted by temperature-dependent factors (Hottel and Sarofim, 1967). In the model, each of the I gray gases has a constant pressure absorption coefficient k_i, and the clear gas has $k_0 = 0$.

$$\varepsilon = \sum_{i=0}^{I} a_{\varepsilon,i}(T_g)(1 - e^{-k_i PL})$$

$$\text{where } a_{\varepsilon,i} = \sum_{j=1}^{J} b_{\varepsilon,i,j} T_g^{j-1} \quad (i = 1, \cdots I) \quad \text{and} \quad a_{\varepsilon,0} = 1 - \sum_{i=1}^{I} a_{\varepsilon,i}$$

(18)

where P, L, and T_g are the sum of the partial pressures of the participating gases, beam length, and gas temperature, respectively.

The Smith et al. (1982) WSGGM has been commonly used in combustion CFD, until new efforts are made recently to properly address the impacts of high-concentration CO_2 and H_2O vapor under oxy-fuel conditions on the gaseous radiative properties (Yin et al., 2010b; Johansson et al., 2011; Kangwanpongpan et al., 2012; Krishnamoorthy, 2013; Bordbar et al., 2014; Guo et al., 2015). In the new models, the variations in H_2O and CO_2 concentrations in a flame are also considered in different ways. Most commonly, discrete coefficient tables are used to address the variations in gas compositions, in the similar way of the Smith et al. (1982) WSGGM. For instance, the oxy-fuel WSGGM (Yin et al., 2010b) accounts for the species variations by using 7 coefficient tables, each of which corresponds to a typical H_2O and CO_2 condition. Based on the local gas composition, different tables are used to evaluate the local radiative properties. The use of discrete coefficient tables may result in discontinuity, i.e., a small change in gas composition may induce a sharp change in the radiative properties. To eliminate the discontinuity problem, smooth coefficient functions of H_2O/CO_2 molar ratio are proposed more recently to address the species variations in a flame (Johansson et al., 2011; Kangwanpongpan et al., 2012; Bordbar et al., 2014; Guo et al., 2015).

Despite of all the progresses in refining WSGGMs, the WSGGMs still have limitations in practical use. For instance, all WSGGMs only account for the impacts of H_2O and CO_2 under atmospheric pressure. In oxy-fuel combustion, CO concentrations can be 10 times higher than that in conventional air-fuel combustion. Although the spectral absorption bands of CO and CO_2 are mostly overlapped, zones of high CO concentrations and high CO_2 concentrations are never overlapped in a real combustor. As a result, excluding CO in the calculation of gaseous radiative properties, as done in WSGGMs, is expected to yield errors in the results. This has been demonstrated in a CFD analysis of a 0.8 MW natural gas oxy-fuel furnace (Yin, 2017), in which a computationally efficient exponential wide band model (E-EWBM) is presented and implemented into the CFD analysis. The Yin et al. (2010b) oxy-fuel WSGGM, which is derived using the EWBM as the reference model, is also implemented into CFD analysis of the same furnace. The simulation results based on the two gaseous radiative property models are compared to each other as well as to the experimental data. The E-EWBM, which can naturally account for H_2O, CO_2, CO, CH_4, NO and SO_2 in the evaluation of gaseous radiative properties, is found to make distinct difference with the oxy-fuel WSGGM in the CFD results, due to the impacts of high-concentration CO in a relatively large zone in the furnace.

The accuracy of the E-EWBM may be further improved by refining some of the model parameters based on the line-by-line calculation with the HITEMP-2010 database, as attempted in (Yan et al., 2015). Such refinements can yield about 6% difference in the total emissivity compared to the original EWBM (Yin, 2016). It needs to be emphasized that the accuracy of a specific CFD-oriented gas radiative property model (including the E-EWBM) can only be assessed by the comparison with the most comprehensive and accurate approach such as the line-by-line approach (Centeno et al., 2015). Besides the E-EWBM, some other models, such as the spectral-line-based weighted-sum-of-gray-gases and the full-spectrum k-distribution method (Modest, 2003), are also practically accurate, computationally competitive and able to address the practical limitations of the WSGGMs. These models are more straightforward in non-gray calculation than the E-EWBM is. As a result, they can also be reliably used in general combustion CFD.

In solid fuel particles, the particles have also strong impacts on radiative heat transfer, as seen in Eq. (2), (4) and (5). In suspension-fired furnaces, in which solid particle concentrations are high, particle radiation can overwhelm gas radiation even under oxy-fuel combustion conditions (Yin, 2015, 2016). As a result, it is important to derive reliable composition-dependent models for particle radiative properties. For instance, instead of the constant particle emissivity and the constant particle scattering factor as commonly used in solid fuel combustion CFD, a conversion degree-dependent particle emissivity and scattering factor can be used as follows (Yin, 2015),

$$\begin{cases} \varepsilon_p = 0.4 \cdot U_C + 0.6 \\ f_p = 0.9 U_{VM,C} + 0.6 (1 - U_{VM,C}) \end{cases} \tag{19}$$

where U_C and $U_{VM,C}$ represents the fraction of unburnt char and the fraction of unburnt combustibles (i.e., volatile matters and char) in a fuel particle, respectively. In effect, the particle emissivity ε_p varies from 1.0 for unburned coal to 0.6 for residual ash. The particle scattering factor changes from 0.9 for unburnt coal (yielding a lower particle scattering coefficient) to 0.6 for residual ash particles (corresponding to a higher particle scattering coefficient), according to Eq. (5).

6.2 Modeling of combustion chemistry under oxy-fuel conditions

The high-concentration CO_2 in oxy-fuel flames has also important chemical effects, via homogeneous and/or heterogeneous reactions, and yields higher CO concentrations (Toftegaard et al., 2010; Chen et al., 2012; Yin and Yan, 2016). H_2O vapor in oxy-fuel combustion also has chemical effects: it can promote or inhibit CO oxidation depending on the specific conditions. Global combustion mechanisms such as the 2-step and 4-step mechanisms presented in section 3.5 are commonly used in combustion CFD due to their good computational efficiency. However, none of them has been validated against oxy-fuel experimental data.

Andersen et al. (2009) refined the 2-step and 4-step global mechanisms for oxy-fuel combustion by using a detailed chemical kinetic mechanism as the reference model. In the refined schemes, the initiating reactions involving hydrocarbon and oxygen are retained while the H_2-CO-CO_2 reactions are modified to improve prediction of the major species concentrations. A comparative CFD analysis of a propane oxy-fuel flame is also made. Comparing to the original versions, the refined WD 2-step mechanism improves the prediction of the temperature field and CO in the post flame zone and the refined JL 4-step mechanism slightly better predicts the CO profile in the flame zone. However, the refined JL 4-step scheme involves $[H_2]^{-0.75}$ in the reaction rate of (R9), which can cause numerical instability or difficulty in CFD simulations, e.g., in the zones without H_2.

In the CFD analysis of a 0.8 MW natural gas oxy-fuel flame, three global mechanisms are compared (Yin et al., 2011): i) the original WD 2-step scheme (Westbrook and Dryer, 1981), ii) the refined WD 2-step scheme (Andersen et al., 2009), and iii) a newly refined JL 4-step scheme. The newly refined JL 4-step mechanism is generated by using the H_2 oxidation model of Marinov et al. (Marinov et al., 1996) to replace the reversible H_2 oxidation reaction (R9) in the original JL 4-step mechanism. The Eddy Dissipation Concept (EDC) is used for turbulence-chemistry interaction. The CFD results of the three computational cases are compared to each other and also against the experimental data. When applied to oxy-fuel combustion, the original WD 2-step scheme is found to over-predict the flame temperature and also largely under-predict the CO level. Both the refined WD 2-step and newly modified JL 4-step schemes can reasonably well predict the relatively high CO level in the furnace, in which the latter also reasonably well predicts H_2 level and flame temperature (Yin et al., 2011).

Recently, Chen and Ghoniem (2014) perform a CFD study of a swirling diffusion flame under air-fuel and oxy-fuel conditions, respectively. It is found the original WD 2-step global mechanism (Westbrook and Dryer, 1981) with either the Eddy Dissipation model or EDC for turbulence-chemistry interaction cannot reasonably predict the CO concentrations. The WD quasi-global mechanism (12 species and 22 reactions)

(Westbrook and Dryer, 1981, 1984) combined with the EDC is found able to capture the chemical effects of CO_2 in oxy-fuel combustion and show improved performance in both air-fuel and oxy-fuel flame CFD simulations.

As recommended in (Yin and Yan, 2016), for large-scale oxy-fuel combustion CFD, the 2-step or 4-step global mechanisms with kinetic parameters refined for oxy-fuel conditions, in combination with the EDC for turbulence-chemistry interaction, can be used. In case of need, more computationally expensive WD multiple-step quasi-global mechanism (12 species and 22 reactions), coupled with the EDC, can also be used. For non-premixed oxy-fuel flame, the mixture fraction method and the steady flamelet chemistry model is also an alternative option.

Oxy-fuel conditions also have important impacts on char reactions. As reviewed and recommended in (Yin and Yan, 2016), char gasification reactions become increasingly important under oxy-fuel conditions due to the elevated concentrations of CO_2 and H_2O. As a result, the traditional single-film model needs to be extended to account for not only char oxidation (R1 and R2) but also char gasification reactions (R3 and R4), in order to appropriately predict the reaction rates and char particle fate.

7. Concluding remarks

CFD modeling of coal and biomass co-firing has been discussed in detail in this chapter, from which the key modeling strategies, modeling issues and the recommendations are summarized in Table 1.

Table 1

As seen in Table 1, new models or refined models still need to be developed for reliable CFD of coal and biomass co-firing. For example, motion and conversion of biomass particles, conversion of the dense fuel bed or a packed fuel bed in fluidized bed or grate

boilers, or gas radiation and gas combustion under oxy-fuel conditions, all need special attention in modeling. More detailed and accurate experimental data are also needed to validate the individual new models as well as various coal/biomass co-firing CFD.

References

Álvarez L, Yin C, Riaza J, Pevida C, Pis JJ, Rubiera F, 2013. Oxy-coal combustion in an entrained flow reactor: Application of specific char and volatile combustion and radiation models for oxy-firing conditions. Energy 62:255–268.

Álvarez L, Yin C, Riaza J, Pevida C, Pis JJ, Rubiera F, 2014. Biomass co-firing under oxy-coal conditions: A computational fluid dynamics modelling study and experimental validation, Fuel Processing Technology 120;22–33.

Al-Mansour F, Zuwala J, 2010. An evaluation of biomass co-firing in Europe. Biomass Bioenerg 34:620–629.

Andersen J, Rasmussen CL, Giselsson T, Glarborg P, 2009. Global combustion mechanisms for use in CFD modeling under oxy-fuel conditions, Energy Fuels 23:1379–1389.

Badzioch S, Hawksley PGW, 1970. Kinetics of thermal decomposition of pulverized coal particles, Ind Eng Chem Process Des Develop 9:521–530.

Baxter LL, 1993. Ash deposition during biomass and coal combustion: a mechanistic approach, Biomass and Bioenergy 4:85–102.

Benyahia S, Syamlal M, O'Brien TJ. Summary of MFIX Equations 2012-1. From URL <https://mfix.netl.doe.gov/download/mfix/mfix_current_documentation/MFIXEquations2012-1.pdf>, January 2012. Accessed October 25, 2017.

Bhuiyan AA, Naser J, 2015. CFD modelling of co-firing biomass with coal under oxy-fuel combustion in a large scale power plant, Fuel 159:150–168.

Bhuiyan AA, Naser J, 2016. Thermal characterization of coal/straw combustion under air/oxy-fuel conditions in a swirl-stabilized furnace: A CFD modelling, Applied Thermal Engineering 93:639–650.

Black S, Szuhánszki J, Pranzitelli A, Ma L, Stanger PJ, Ingham DB, Pourkashanian M, 2013. Effects of firing coal and biomass under oxy-fuel conditions in a power plant boiler using CFD modelling, Fuel 113:780–786.

Blasiak W, Yang WH, Dong W, 2006. Combustion performance improvement of grate fired furnaces using Ecotube system, J Energy Inst 79:67–74.

Bordbar MH, Wecel G, Hyppänen T, 2014. A line by line based weighted sum of gray gases model for inhomogeneous CO_2–H_2O mixture in oxy-fired combustion, Combust Flame 161: 2435–2445.

Centeno FR, Brittes R, Franca FHR, Ezekoye OA, 2015. Evaluation of gas radiation heat transfer in a 2D axisymmetric geometry using the line-by-line integration and WSGG models, J Quant Spectrosc Radiat Transf 156:1–11.

Chen L, Yong SZ, Ghoniem AF, 2012. Oxy-fuel combustion of pulverized coal: Characterization, fundamentals, stabilization and CFD modeling, Prog Energy Combust Sci 38:156–214.

Chen L, Ghoniem, AF, 2014. Modeling CO_2 chemical effects on CO formation in oxy-fuel diffusion flames using detailed, quasi-global, and global reaction mechanisms, Combust Sci Technol 186:829–848.

Chui EH, Hughes PMJ, Raithby GD, 1993. Implementation of the finite volume method for calculating radiative transfer in a pulverized fuel flame. Combust Sci Technol 92:225–242.

Collazo J, Porteiro J, Patiño D, Granada E, 2012. Numerical modeling of the combustion of densified wood under fixed-bed conditions, Fuel 93:149–159.

Costa M, Massarotti N, Indrizzi V, Rajh B, Yin C, Samec N, 2014. Engineering bed models for solid fuel conversion process in grate-fired boilers, Energy 77:244–253.

De Soete GG, 1975. Overall reaction rates of NO and N_2 formation from fuel nitrogen. Proc Combust Inst 15:1093–1102.

Glarborg P, Jensen AD, Johnsson JE, 2003. Fuel nitrogen conversion in solid fuel fired systems, Prog Energy Combust Sci 29:89–113.

Goddard CD, Yang YB, Goodfellow J, Sharifi VN, Swithenbank J, Chartier J, et al., 2005. Optimisation study of a large waste-to-energy plant using computational modelling and experimental measurements, J Energy Inst 78:106–116.

Goerner K, Klasen T, 2006. Modelling, simulation and validation of the solid biomass combustion in different plants, Progr Comput Fluid Dyn 6:225–234.

Gómez MA, Porteiro J, Patiño D, Míguez JL, 2014. CFD modelling of thermal conversion and packed bed compaction in biomass combustion, Fuel 117:716–732.

Grant DM, Pugmire RJ, Fletcher TH, Kerstein AR, 1989. Chemical percolation model of coal devolatilization using percolation lattice statistics, Energy Fuels 3:175–186.

Guo J, Li X, Huang X, Liu Z, Zheng C, 2015. A full spectrum k-distribution based weighted-sum-of-gray-gases model for oxy-fuel combustion, Int J Heat Mass Transf 90:218–226.

Hill SC, Smoot LD, 2000. Modeling of nitrogen oxides formation and destruction in combustion systems, Prog Energy Combust Sci 26:417–458.

Hottel HC, Sarofim AF, 1967. Radiative Transfer, New York, McGraw-Hill.

IEA: Bioenergy Agreement Task32 (website). www.ieabcc.nl/database/cofiring.php. Accessed October 25, 2017.

Johansson R, Thunman H, Leckner B, 2007. Sensitivity analysis of a fixed bed combustion model, Energy Fuels 21:1493–1503.

Johansson R, Leckner B, Andersson K, Johnsson F, 2011. Account for variations in the H_2O to CO_2 molar ratio when modeling gaseous radiative heat transfer with the weighted-sum-of-grey-gases model, Combust Flame 158:893–901.

Jones WP, Lindstedt RP, 1988. Global reaction schemes for hydrocarbon combustion, Combust Flame 73:233–249.

Kangwanpongpan T, França FHR, da Silva RC, Schneider PS, Krautz HJ, 2012. New correlations for the weighted-sum-of-gray-gases model in oxy-fuel conditions based on HITEMP 2010 database, Int J Heat Mass Transf 55:7419–7433.

Kim S, Shin D, Choi S, 1996. Comparative evaluation of municipal solid waste incinerator designs by flow simulation, Combust and Flame 106:241–251.

Kitto JB, Stultz SC. Steam: its generation and use. 41st ed. Ohio: The Babcock & Wilcox Company; 2005.

Klason T, Bai XS, 2006. Combustion process in a biomass grate fired industry furnace: a CFD study, Progr Comput Fluid Dyn 6:278–82.

Kobayashi H, Howard JB, Sarofim AF, 1976. Coal devolatilization at high temperatures, Proc Combust Inst 16:411–425.

Krishnamoorthy G, 2013. A new weighted-sum-of-gray-gases model for oxy-combustion scenarios, Int J Energy Res 37:1752–1763.

Kær SK, 2004. Numerical modelling of a straw-fired grate boiler, Fuel 83:1183–1190.

Kær SK, Rosendahl LA, Baxter LL, 2006. Towards a CFD-based mechanistic deposit formation model for straw-fired boilers, Fuel 85:833–848.

Lavery P. Combustion industry news – From the IFRF's correspondent in Australia, 2013 (website). www.mnm.ifrf.net/mnm/article.html?aid=1174. Accessed October 25, 2017.

Lee FCC, Lockwood FC, 1999. Modelling ash deposition in pulverized coal-fired applications, Progress in Energy and Combustion Science 25:117–132.

Lockwood FC, Romo-Millares CA, 1992. Mathematical modeling of fuel–NO emissions from PF burners, J Inst Energy 65:144–152.

Mandø M, Rosendahl L, Yin C, Sørensen H, 2010. Pulverized straw combustion in a low-NO_x multi-fuel burner: modeling the transition from coal to Straw, Fuel 89:3051–3062.

Marinov NM, Westbrook CK, Pitz WJ, 1996. Detailed and global chemical kinetics model for hydrogen. In Chan SH (Ed.) Transport phenomena in combustion. Washington DC, Taylor and Francis.

Maxey MR, Riley JJ, 1983. Equation of motion for a small rigid sphere in a nonuniform flow, Physics of Fluids 26:883–889.

Miller JA, Bowman CT, 1989. Mechanism and modeling of nitrogen chemistry in combustion, Prog Energy Combust Sci 15:287–338.

Modest MF, 2003. Radiative heat transfer, ed 2, New York, Academic Press.

Nasserzadeh V, Swithenbank J, Jones B, 1991. Three-dimensional modelling of a municipal solid-waste incinerator, J Inst Energy 64:166–175.

Nasserzadeh V, Swithenbank J, Jones B, 1993. Effect of high speed secondary air jets on the overall performance of a large MSW incinerator with a vertical shaft, Combust Sci Technol 92:389–422.

Niksa S, Kerstein AR, 1991. FLASHCHAIN theory for rapid coal devolatilization kinetics. 1. Formulation, Energy Fuels 5:647–665.

Olenik G, Stein OT, Kronenburg A, 2015. LES of swirl-stabilised pulverised coal combustion in IFRF furnace no. 1, Proceedings of the Combustion Institute 35:2819–2828.

Pitsch H, 2006. Large-eddy simulation of turbulent combustion, Annu Rev Fluid Mech 38:453–482.

Rabacal M, Franchetti BM, Marincola FC, Proch F, Costa M, Hasse C, Kempf AM, 2014. LES of coal combustion in a large-scale laboratory furnace, Proceedings of the Combustion Institute 35:2609–3617.

Rajh B, Yin C, Samec N, Hribersek M, Zadravec M, 2016. Advanced modelling and testing of a 13 MW_{th} waste wood-fired grate boiler with recycled flue gas, Energy Conversion and Management 125:230–241.

Rosendahl L, Yin C, Kær SK, Friborg K, Overgaard P, 2007. Physical characterization of biomass fuels prepared for suspension firing in utility boilers for CFD modeling, Biomass & Bioenergy 31:318–325.

Ryu C, Shin D, Choi S, 2002. Combined simulation of combustion and gas flow in a grate-type incinerator, J Air Waste Manage Assoc 52:174–185.

Ryu C, Yang YB, Nasserzadeh V, Swithenbank J, 2004. Thermal reaction modelling of a large municipal solid waste incinerator, Combust Sci Technol 176:1891–1907.

Shin D, Choi S, 2000. The combustion of simulated waste particles in a fixed bed, Combust Flame 121:167–180.

Smith TF, Shen ZF, Friedman JN, 1982. Evaluation of coefficients for the weighted sum of gray gases model, J Heat Transf–Trans ASME 104:602–608.

Solomon PR, Hamblen DG, Carangelo RM, Serio MA, Deshpande GV, 1988. General model of coal devolatilization, Energy Fuels 2:405–422.

Stubenberger G, Scharler R, Zahirovic S, Obernberger I, 2008. Experimental investigation of nitrogen species release from different solid biomass fuels as a basis for release models, Fuel 87:793–806.

Thunman H, Leckner B, 2005. Influence of size and density of fuel on combustion in a packed bed, Proc Combust Inst 30:2939–2946.

Toftegaard MB, Brix J, Jensen PA, Glarborg P, Jensen AD, 2010. Oxy-fuel combustion of solid fuels, Prog Energy Combust Sci 36:581–625.

Wang H, Harb JN, 1997. Modeling of ash deposition in large-scale combustion facilities burning pulverized coal, Progress in Energy and Combustion Science 23:267–282.

Weber R, Mancini M, Schaffel-Mancini N, Kupka T, 2013. On predicting the ash behavior using Computational Fluid Dynamics, Fuel Processing Technology 105:113–128.

Weissinger A, Fleckl T, Obernberger I, 2004. In situ FT-IR spectroscopic investigations of species from biomass fuels in a laboratory-scale combustor: the release of nitrogenous species, Combust Flame 137:403–417.

Westbrook CK, Dryer FL, 1981. Simplified reaction-mechanisms for the oxidation of hydrocarbon fuels in flames, Combust Sci Technol 27:31–43.

Westbrook CK, Dryer FL, 1984. Chemical kinetic modeling of hydrocarbon combustion, Prog Energy Combust Sci 10:1–57.

Yan L, Yue G, He B, 2015. Development of an absorption coefficient calculation method potential for combustion and gasification simulation, Int J Heat Mass Transf 91:1069–1077.

Yang YB, Ryu C, Khor A, Yates NE, Sharifi VN, Swithenbank J, 2005. Effect of fuel properties on biomass combustion. Part II. Modelling approach – Identification of the controlling factors, Fuel 84:2116–2130.

Yang YB, Newman R, Sharifi V, Swithenbank J Ariss J, 2007. Mathematical modelling of straw combustion in a 38MWe power plant furnace and effect of operating conditions, Fuel 86:129–142.

Yin C, Rosendahl L, Kær SK, Sørensen H, 2003. Modelling the motion of cylindrical particles in a nonuniform flow, Chemical Engineering Science 58:3489–3498.

Yin C, Rosendahl L, Kær SK, Condra T, 2004. Use of numerical modeling in design for co-firing biomass in wall-fired burners, Chemical Engineering Science 59:3281–3292.

Yin C, Rosendahl L, Kær SK, 2008a. Grate-firing of biomass for heat and power production, Progress in Energy and Combustion Science 34:725–754.

Yin C, Rosendahl L, Kær SK, Clausen S, Hvid SL, 2008b. Mathematical modeling and experimental study of biomass combustion in a thermal 108 MW grate-fired boiler, Energy & Fuels 22:1380–1390.

Yin C, Kær SK, Rosendahl L, Hvid SL, 2010a. Co-firing straw with coal in a swirl-stabilized dual-feed burner: modeling and experimental validation, Bioresource Technology 101:4169–4178.

Yin C, Johansen LCR, Rosendahl L., Kær SK, 2010b. A new weighted sum of gray gases model applicable to CFD modeling of oxy-fuel combustion: derivation, validation and implementation, Energy Fuels 24:6275–6282.

Yin C, Rosendahl L, Kær SK, 2011. Chemistry and radiation in oxy-fuel combustion: A computational fluid dynamics modeling study, Fuel 90:2519–2529.

Yin C, Rosendahl L, Clausen S, Hvid SL, 2012. Characterizing and modeling of an 88 MW grate-fired boiler burning wheat straw: Experience and lessons, Energy 41:473–482.

Yin C, 2015. On gas and particle radiation in pulverized fuel combustion furnaces, Applied Energy 157:554–561.

Yin C, 2016. Effects of moisture release and radiation properties in pulverized fuel combustion: A CFD modelling study, Fuel 165:252–259.

Yin C, Yan J, 2016. Oxy-fuel combustion of pulverized fuels: Combustion fundamentals and modeling, Applied Energy 162:742–762.

Yin C, 2017. Prediction of air-fuel and oxy-fuel combustion through a generic gas radiation property model, Applied Energy 189:449–459.

Yin C, Li S, 2017. Advancing grate-firing for greater environmental impacts and efficiency for decentralized biomass/waste combustion, Energy Procedia 120:373–379.

Yu J, Lucas JA, Wall TF, 2007. Formation of the structure of chars during devolatilization of pf pulverized coal and its thermoproperties: a review. Prog Energy Combust Sci 33:135–170.

Zeldovich YB, 1946. The oxidation of nitrogen in combustion and explosions, Acta Physicochem USSR 21:577–628.

Zhou H, Jensen AD, Glarborg P, Jensen PA, Kavaliauskas A, 2005. Numerical modeling of straw combustion in a fixed bed, Fuel 84:389–403.

Zhou H, Jensen PA, Frandsen FJ, 2007. Dynamic mechanistic model of superheater deposit growth and shedding in a biomass fired grate boiler, Fuel 86:1519–1533.
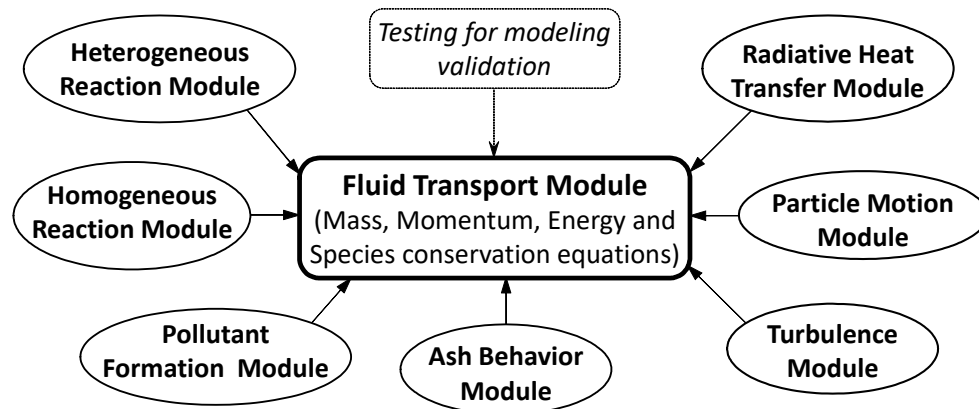
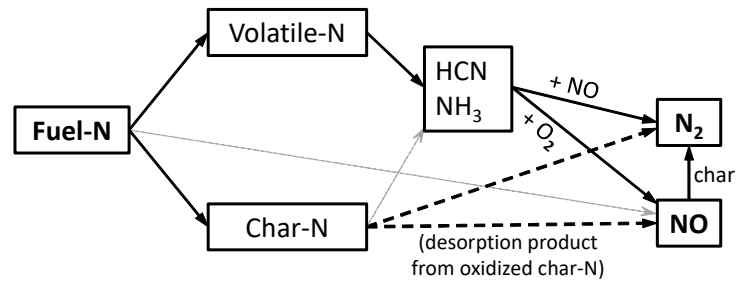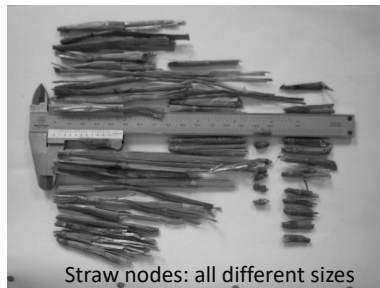Figure 1. CFD modeling of coal and biomass co-firing: An overview of the basic modules

Figure 2. Fuel-N conversion (soot and soot-N conversion neglected)

Figure 3. Straw particle samples collected prior to injection into the furnace

Wood pellets
(commercially available)

Milled samples

d_p=**2** mm

Roller-milled

d_p=**3** mm

Roller-milled

Roller-milled wood pellet samples, collected from a transport pipe to a burner in a co-firing plant
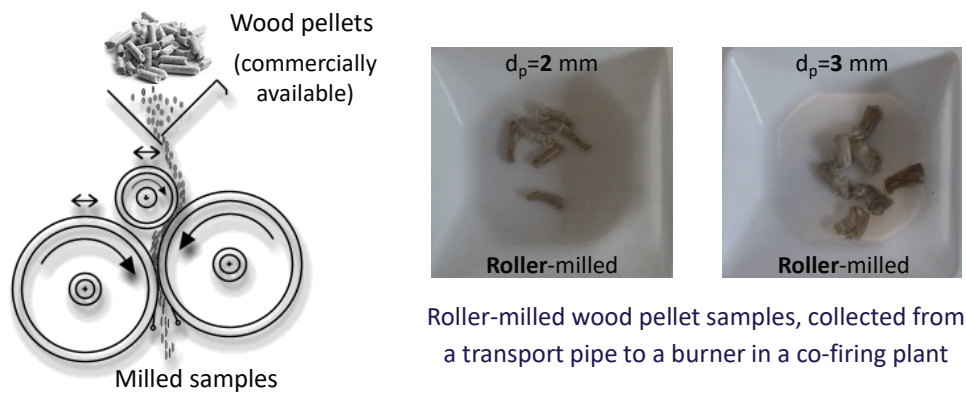
Figure 4. Roller milling of wood pellets and the milled samples

Wood pellets

Milled samples

d_p=**2** mm **Hammer**-milled

d_p=**3** mm **Hammer**-milled

Hammer-milled wood pellet samples,
collected from hammer-mill trials
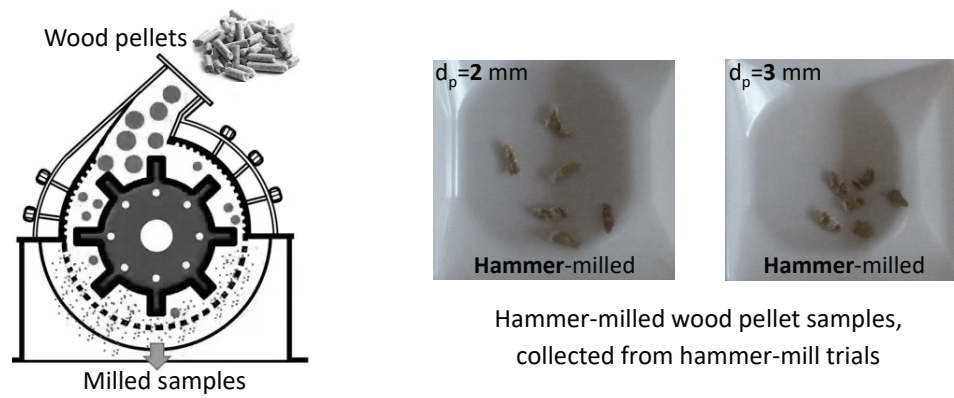
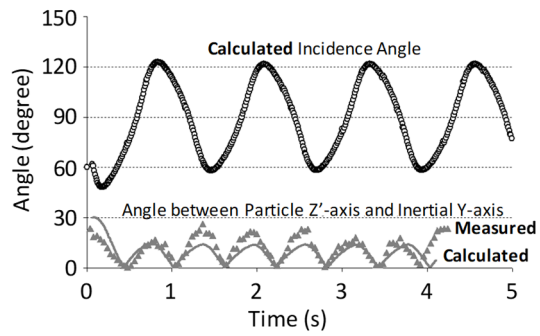Figure 5. Hammer milling of wood pellets and the milled samples
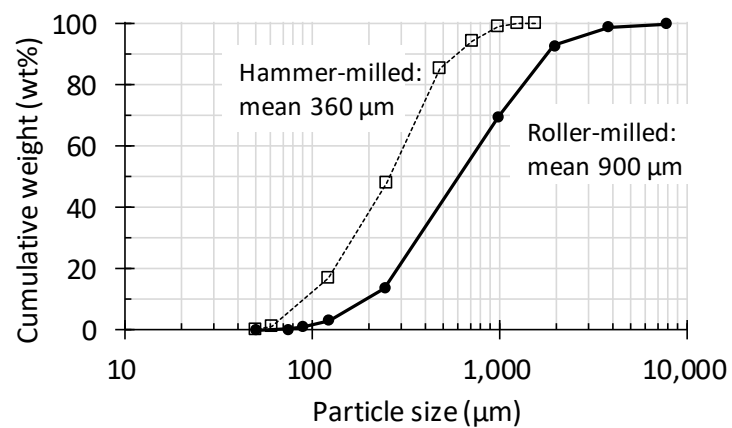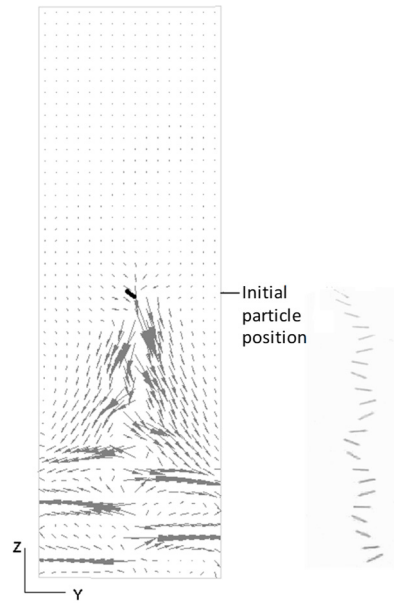
Figure 6. Cumulative particle size distribution of the biomass pellet samples ground by a conventional coal roller mill and by a hammer mill, respectively
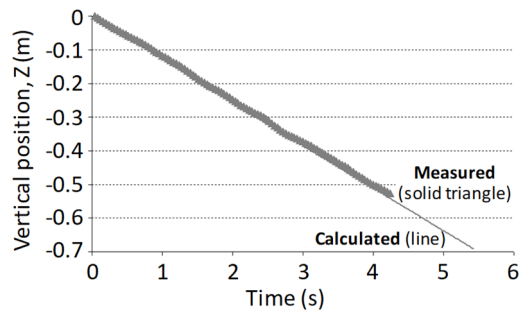
(a) Translation motion

(b) Rotation motion

(c) Final water flow pattern and the particle trajectory

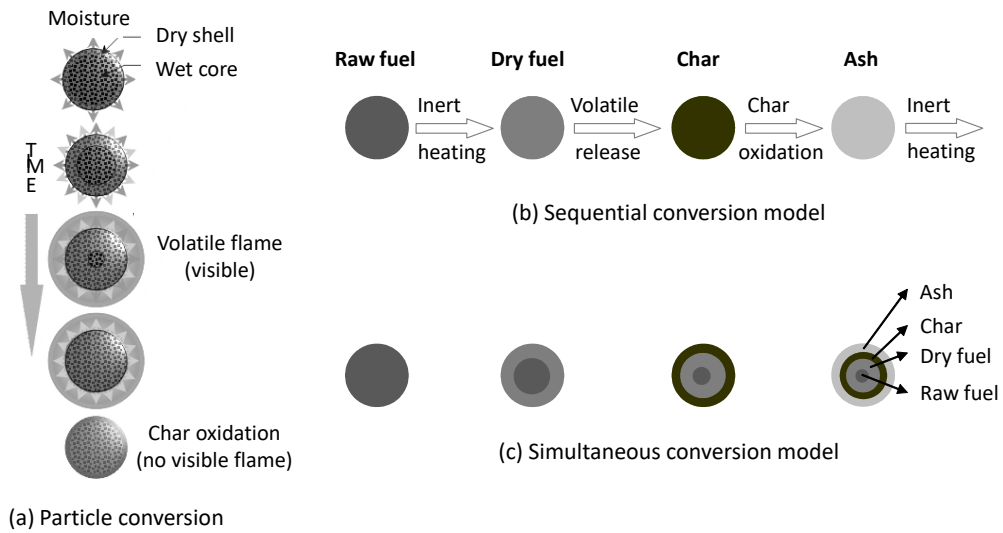Figure 7. Motion of a large cylindrical PVC particle in originally stagnant water

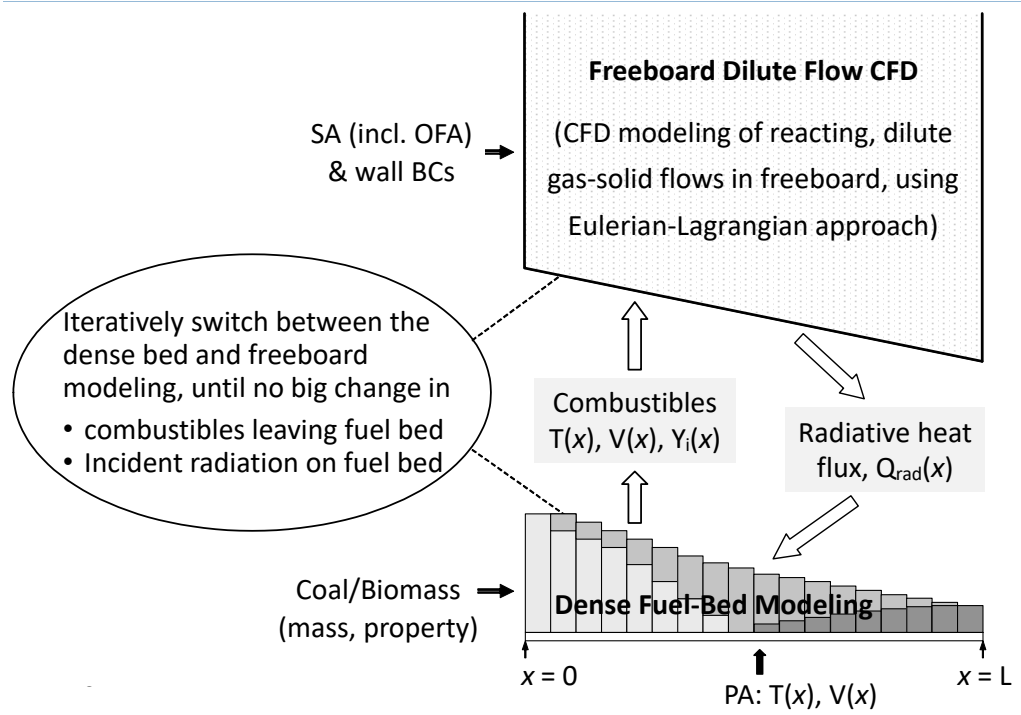Figure 8. Different solid fuel particle conversion patterns

Figure 9. Coupled modeling strategy for co-firing in fluidized bed or grate boilers

Table 1. CFD of coal and biomass co-firing: A handy summary and recommendation.

1) Modeling of pulverized fuel combustion in general: Coupled Eulerian-Lagrangian, in which fluid equations are solved in Eulerian framework and solid particles are tracked in Lagrangian framework, with key modeling issues summarized below.

Turbulence	Realizable k-ε or Reynolds stress model recommended for industrial combustion CFD. If computationally affordable, LES preferred.
Particle motion	Equation of motion including both drag and gravity forces.
Radiation heat transfer	Discrete Ordinates model preferred (or P1 for industrial boilers); WSGGM for gaseous radiative properties; conversion degree-dependent particle radiative properties.
Heterogeneous reactions	i) Pyrolysis: single kinetic rate model, with Arrhenius parameters preferably determined by experiments; ii) Char reactions: single-film model with char oxidation reactions.
Homogeneous reactions	2-step or 4-step mechanisms, with EDC for turbulence-chemistry interaction (for non-premixed combustion: mixture fraction/PDF also a good option).
NO_x emissions	Thermal and fuel NO_x, with attention to fuel NO_x (e.g., split of fuel-N in volatiles and char, split of volatile-N in different precursors).
Ash deposition	Inertial impacts of fly ash particles and key shedding factors both to be correctly considered and implemented.

2) Suspension co-firing of coal and biomass: Specific modeling issue

Particle motion	Extended equation of motion for coupled translation and rotation, for new motion patterns of large, non-spherical biomass particles
Particle conversion	Simultaneous conversion model for large biomass particle, instead of sequential conversion model for tiny pulverized coal particle

3) Grate and/or fluidized bed co-firing of coal and biomass: Specific modeling issue

Overall method	Coupled dense fuel bed conversion modeling and freeboard CFD
Dense fuel bed	New modeling effort needed for dense fuel bed conversion

4) Co-firing of coal and biomass under oxy-fuel conditions: New modeling issues

Gas radiation	New model needed to properly account for the impacts of high-concentration CO, CO_2 and H_2O in oxy-fuel furnaces
Gas phase combustion	Refined global combustion mechanisms for oxy-fuel, to address the chemical effects of high-concentrations CO_2 and H_2O
Char reactions	Extended single-film model with all the char oxidation and gasification reactions